J Mater Sci (2011) 46:6925–6931
DOI 10.1007/s10853-011-5658-6

Structural, optical and electrical measurements on boron-doped CdO thin films

A. A. Dakhel

Received: 31 March 2011 / Accepted: 24 May 2011 / Published online: 4 June 2011

Abstract Several boron-doped CdO with different boron composition thin films have been prepared on glass substrate by a vacuum evaporation technique. The effects of boron doping on the structural, electrical and optical properties of the host CdO films were systematically studied. The X-ray diffraction study shows that some of B^{3+} ions occupied locations in interstitial positions and/or Cd^{2+}-ion vacancies of CdO lattice. The band gap of B-doped CdO suffers narrowing by 30–38% compare to undoped CdO. Such band gap narrowing (BGN) was studied in the framework of the available models. Furthermore, a phenomenological evaluation of the dependence of band gap on the carrier concentration in the film samples is discussed. The electrical behaviours show that all the prepared B-doped CdO films are degenerate semiconductors. However, the boron doping influences all the optoelectrical properties of CdO. Their dc-conductivity, carrier concentration and mobility increase compare to undoped CdO film. The largest mobility of 45–47 cm^2/V s was measured for 6–8% boron-doped CdO film. From near infrared transparent-conducting oxide (NIR-TCO) point of view, boron is effective for CdO donor doping.

Introduction

Cadmium oxide CdO has a wide range of applications in optoelectronics like transparent conducting oxide (TCO), solar cells, optical communications, photo-transistors, as well as other type of applications like IR heat mirror, gas sensors, low-emissive windows,… etc. [1–3]. These applications stand on its degenerate semiconducting electrical and optical properties. Donor states in non-stoichiometric CdO arising from cadmium interstitials or oxygen vacancies give rise to a well-defined impurity band, which grows and merges with the conduction band [4]. Therefore, non-stoichiometric CdO has n-type semiconducting behaviour with relatively low electrical resistivity (10^{-2} to 10^{-4} Ω cm). Furthermore, CdO films are transparent in visible and NIR spectral regions with a direct band gap of 2.2–2.7 eV [1, 5, 6]. CdO crystallises in a cubic structure of space group Fm3m of 6-coordination of a lattice constant of 0.4695 nm [7].

The optoelectronic properties of CdO could be controlled by doping with different metallic ions such as Sn [1, 3], In, Y [4], Tl [8], Al [9], Sc [10], Fe [11], Sm [12], Dy [13], etc. It was observed that when the size of the dopant ion is slightly smaller than that of Cd^{2+}, then the resistivity of the doped CdO film decreases and the lattice unit cell compresses. However, the doping by any technique of CdO with ions of smaller radius like boron was not yet investigated, although such doping was conducted for other TCO's like ZnO [14–16], SnO_2 [17], In_2O_3 [18] and NiO [19]. The 6-coordination ionic radius of B^{3+} is 0.027 nm, which is much smaller than that of Cd^{2+} ion, 0.095 nm [20]. This study reports the effect of boron heavy doping on the structural, electrical and optical properties of CdO. It will be seen that boron doping of CdO is efficient for obtaining high mobility and conductivity in comparison with other dopants and could be successfully used for technical applications based on its IR-TCO characteristics. In addition, it is useful to mention here that cadmium borates are of a considerable interest because they are interesting host material for luminescent applications when doped with transition metals or rare earth ions [21].

A. A. Dakhel (✉)
Department of Physics, College of Science, University of Bahrain, P.O. Box 32038, Sakhier, Kingdom of Bahrain
e-mail: adakhil@sci.uob.bh

Experimental details

Four sets of CdO thin films incorporated with different amount of boron were grown on glass substrate. It was used as silicon wafer substrates only for SEM study. The starting materials were pure B_2O_3 and CdO (from Fisher sci. company/USA and Fluka A.G./Germany, respectively). The deposition procedure by vacuum evaporation technique has been described elsewhere [12, 13]. The starting materials were evaporated alternatively (layer-by-layer) by alumina baskets (Midwest tungsten service, USA). The substrates were ultrasonically clean glass slides and chemically (using HF) cleaned silicon wafer held in a vacuum chamber of residual oxygen atmosphere of about 1.3×10^{-3} Pa. The as-grown films were totally oxidised and stabilised by flash annealing in air at 400 °C for 2 h keeping samples inside the closed furnace for slow cooling to room temperature. All samples were prepared in almost same conditions including the reference pure CdO film. The evaporated masses were controlled with a piezoelectric microbalance crystal sensor of a Philips FTM5 thickness monitor fixed close to the substrate. The thicknesses were measured after annealing by an MP100-M spectrometer (Mission Peak Optics Inc, USA), to be 0.16–0.2 μm. The surface microtopography and weight ratios of boron to Cd (r) were measured with SEM/EDX microscope (Zeiss EVO). The values of r were 4.8, 6.3, 7.9 and 10% (with the experimental error of about 1.3%, as determined by the SEM software), and accordingly the samples were named as S4.8% B, S6.3% B, S7.9% B and S10% B. The structures of the prepared films were studied by X-ray diffraction (XRD) method using a Philips PW 1710 θ–2θ system with a Cu K_α radiation (0.15406 nm) and a step of 0.02°. The spectral optical transmittance $T(\lambda)$ and reflectance $R(\lambda)$ were measured at normal incidence in UV–Vis–NIR spectral region (400–3000 nm) with a Shimadzu UV-3600 double beam spectrophotometer. The electrical properties were investigated by Hall measurement in the Van der Pauw configuration at room temperature with aluminium dot contacts in a magnetic field of about 1 T and using a Keithley 195A digital multimeter and a Keithley 225 current source

Results and discussion

Structural characterisation

Figure 1a shows the XRD patterns of the prepared undoped and boron-doped CdO films on glass substrates. The patterns of Fig. 1a reveal that all the investigated B-doped CdO samples are polycrystalline with cubic Fm3m CdO structure, as given in Ref. [7]. Boron oxide B_2O_3 peaks [22, 23] were not detected in the XRD pattern of B-doped CdO due to the low B-dopant concentration and to the solid solution formed. Furthermore, peaks belong to any Cd–B–O compound were not detected referring to the absent of any formed compound in the samples. (In the $CdO–B_2O_3$ system, at least three compounds have been proposed [24], including $Cd_3B_2O_6$ (or $3CdO{\cdot}B_2O_3$) [21, 25], $Cd_2B_2O_5$ (or $2CdO{\cdot}B_2O_3$) [26] and CdB_4O_7 (or $CdO{\cdot}2B_2O_3$) [27]).

The films grown on glass substrate have [111] preferred orientation growth, which is usual energetically preferred growth of CdO films prepared by different techniques. The mean X-ray crystallite size (CS) was estimated from the intense (111) reflection using Scherrer equation [28]: $CS = 0.9\lambda/\beta\cos\theta$, where λ is the X-ray wavelength (0.1540 nm); β is the full-width at half maximum (FWHM) of the diffraction peak in radian; and θ corresponds to the peak position. The CS was 34.7 nm for undoped CdO film that grew to about 46.3 nm under boron doping. Thus,

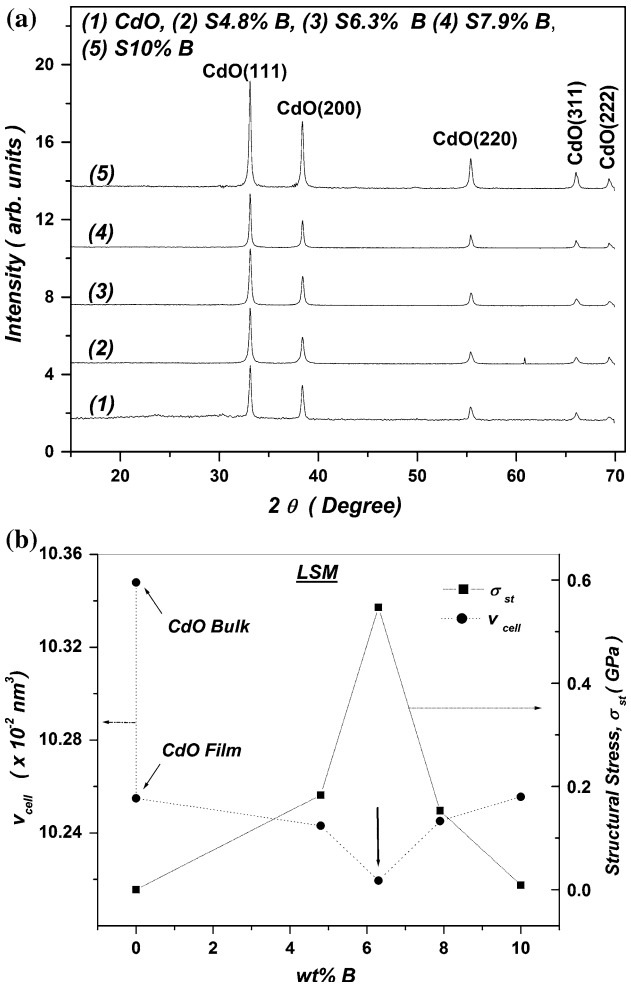

Fig. 1 **a** X-ray diffraction patterns for undoped and B-doped CdO films deposited on glass substrates. **b** Variation of the unit-cell volume (v_{cell}) and structural micro-stress of (σ_{st}) B-doped CdO films deposited on glass substrates

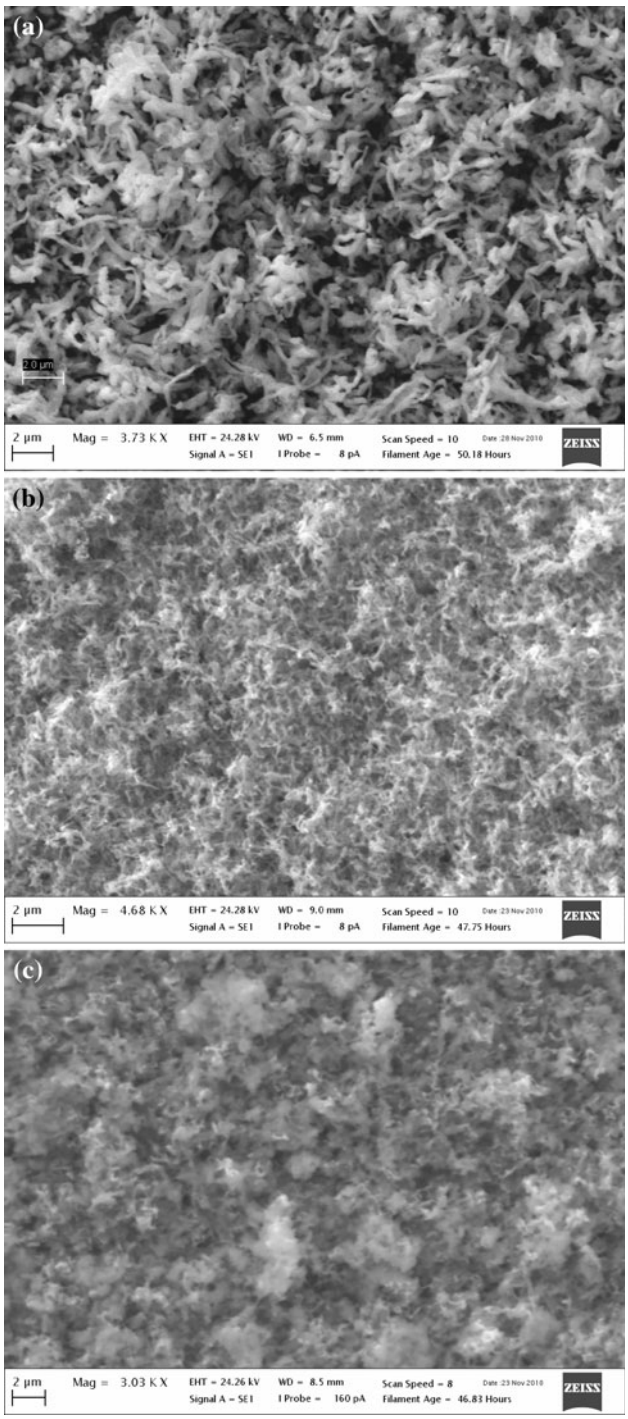

Fig. 2 SEM micrographs of **a** undoped CdO, **b** 4.8% B-doped CdO and **c** 10% B-doped CdO films grown on silicon substrate

compared to that of undoped CdO sample, the crystalline size of CdO increased by boron doping, and the change in doping level has no considerable effect on the CS. Therefore, the prepared samples were nano-crystallite films.

Figure 2 shows the SEM micrographs of un-doped CdO (Fig. 2a), 4.8% B-doped (Fig. 2b) and 10% B-doped (Fig. 2c) CdO films grown on silicon substrate. It can be seen that pure CdO film has non-blowzy wool shape microtopography. This structure gradually transforms to cloudy, as seen in 4.8 and 10% B CdO.

Table 1 Lattice parameter (a), strain (ε_s) and stress (σ_{st}) of the prepared undoped and B-doped CdO films grown on glass substrates

Sample	a (nm)	ε_s ($\times 10^{-3}$)	σ_{st} (GPa)
Powder	0.46948	–	–
CdO	0.46806	–	–
S4.8% B	0.46789	−1.06	0.17
S6.3% B	0.46753	−3.36	0.53
S7.9% B	0.46792	−0.87	0.14
S10% B	0.46808	−0.15	0.02

The lattice parameter (a) and unit-cell volume (v_{cell}) of the host CdO film structure grown on glass substrate are calculated by least squares method (LSM) and the results are given in Table 1 and Fig. 1b. It is observed that the unit-cell volume of the undoped CdO film is smaller than that of the bulk pressed powder disc, due to the creation of structural vacancies inside the crystalline structure (non-stoichiometric composition).

In spite of few number of data points, Fig. 1b reflects the trend of actual doping process of boron into CdO lattice. The B-doping increases with increasing of %boron incorporation until around 6.3% then it decreases, which means that some of the incorporated boron accumulates on the crystallite boundaries. Doping of B^{3+} ions in the host CdO lattice decreases the unit-cell volume since B^{3+} ions have smaller size than that of Cd^{2+} and thus they have high diffusivity with low activation energy. The dissolution of B^{3+} ions in CdO lattice can be realised by substitution for Cd^{2+} ions and/or occupying locations in interstitial positions. For both cases, v_{cell} decreases with B^{3+} doping. However, the B^{3+} substitution for Cd^{2+} ions unlikely happens according to Hume-Rothery rules. According to the Hume-Rothery rules, the solid solution of boron and cadmium oxides unlikely occurs since the radius of the host Cd^{2+} and substitutional B^{3+} ions are different by more than 25%, in addition to that the two ions have different valencies and electronegativities. Thus, the conditions do not preferred the formation of solid solutions. Therefore, the occupation of locations in interstitial positions of CdO lattice with B^{3+} $\left(B_i^{\bullet\bullet\bullet}\right)$ ions is most likely happen. Such doping disturbs the charge neutrality of the unit cell that can be settled by creation of Cd^{2+} ion vacancies $(V_{Cd}^{\bullet\bullet})$ or by leaving some of Cd^{2+} ions to their positions that would reduces the v_{cell}. The B^{3+} ions that occupy interstitial positions might move by the thermal motion, small size and high diffusivity and occupy Cd^{2+}-ion vacancies

($V_{Cd}^{\bullet\bullet}$). In Kroger–Vink notations, the defect reaction is $B_2O_3 \xrightarrow{CdO} V_{Cd}^{x\bullet\bullet} + e' + B_i^{\bullet\bullet\bullet}$ where $V_{Cd}^{x\bullet\bullet}$ is the cadmium-ion Cd^{2+} vacancy of neutral charge, $B_i^{\bullet\bullet\bullet}$ is the boron interstitial ion of triple-positive charge and e' is an electron (a site is not normally specified).

The change in unit-cell volume of B-doped CdO (Δv_{cell}) compare to that of pure CdO $\left(v_{cell}^0\right)$ can be used to calculate the structural strain: $\varepsilon_s = \Delta v_{cell}/v_{cell}^0$; the results are given in Table 1, which is of order -10^{-4} to -10^{-3}. This strain is caused by a compressive stress (σ_{st}) that can be estimated by $\sigma_{st} = \varepsilon_s B$, where B is the average bulk modulus of CdO, which is about 158 GPa [29] and the results are given in Table 1 and Fig. 1b (The negative sign refers to the compression nature of the stress). However, the created stress is far to be capable of creating a crystal-structural transformation, it can only produce a slight decrease in the lattice constant of order about -0.3%.

DC-electrical properties

The room temperature electrical resistivity (ρ), mobility (μ_{el}) and carrier concentration (N_{el}) were measured for undoped and all B-doped CdO films grown on glass substrates by a standard Van der Pauw method, and the average results are presented in Table 2. The experimental error due to the aluminium contact spot size was estimated to be about 5%. The electrical measurements show that the undoped and all B-doped CdO sample (Pure CdO, 4.8, 6.3, 7.9 and 10 wt% B) are n-type semiconductors. The present measurements of N_{el} and μ_{el} for the undoped CdO film agree with the previous published data for CdO films prepared by different techniques [1]. However, the measured resistivity of the undoped CdO film is larger than those values mentioned in some other previous references $\sim 10^{-3}$ to 10^{-4} Ω cm [1] due to different methods and procedures of preparation. In general, the results show that the doping with boron strongly improves all its electrical conduction parameters (ρ, N_{el} and μ_{el}). With increase in doping level, the resistivity of the CdO film decreases from 10^{-2} to 10^{-4} Ω cm, and attains a minimum value at 7.9% B, as shown in Fig. 3. For higher doping levels, the resistivity increases due to a considerable accumulation of boron ions (or boron oxide) on the crystallite boundaries. The utmost improvement of conduction parameter takes place with sample S7.9% B; the conductivity increases by about 130 times, mobility by about 7 times and electronic concentration by about 15 times in comparison to pure CdO film. For a comparison, the increase of conduction parameters was also observed in Ref. [18] by boron implantation in In_2O_3 films. However, these results can be explained as consequence of B^{3+} ions doping by occupation interstitial sites in CdO lattice $\left(B_i^{\bullet\bullet\bullet}\right)$ due to its smaller ion radius and high mobility; such explanation was also adopted in Ref. [14]. As mentioned above, due to the charge balance rule, the formation of $B_i^{\bullet\bullet\bullet}$ must accompanied with the creation of Cd^{2+} vacancies. The growth of $B_i^{\bullet\bullet\bullet}$provide more conduction electrons. Thus, B-doping create donors that improve the conduction and induce band evolve, which merges with the conduction band and reduces the band gap, as will be seen later. Indeed, identical explanation was adopted by other researchers on ZnO [30].

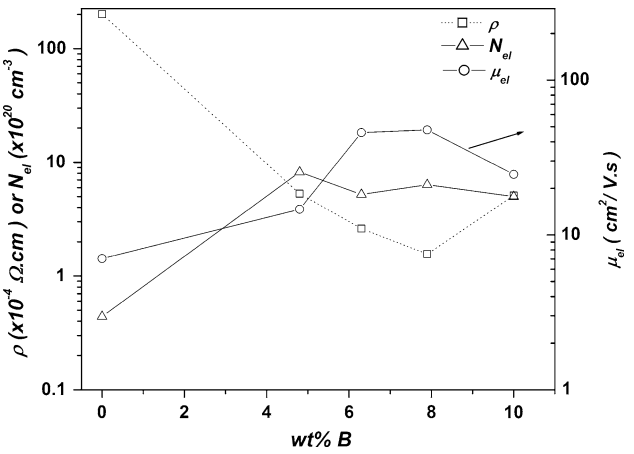

Fig. 3 Variation of resistivity (ρ), mobility (μ_{el}) and carrier concentration (N_{el}) with doping level of B-doped CdO films grown on glass substrate

Table 2 The measured electrical parameters [resistivity (ρ), mobility (μ_{el}) and carrier concentration (N_{el})], band gap (E_g) and absorption coefficient at 2000 nm of undoped and B-doped CdO films grown on glass substrate

Sample	ρ ($\times 10^{-4}$ Ω cm)	μ_{el} (cm^2/V s)	N_{el} (10^{20} cm^{-3})	E_g (eV)	$(N_{el}/\mu_{el})_{el}$	$(N_{el}/\mu_{el})_{op}$	α ($\times 10^4$ cm^{-1})
CdO	201	7.03	0.44	2.42	0.63	0.32	0.2348
S4.8% B	5.3	14.64	8.2	1.58	5.60	5.34	4.4234
S6.3% B	2.61	45.84	5.22	1.68	1.14	4.97	4.6313
S7.9% B	1.56	47.7	6.35	1.58	1.33	3.69	5.1265
S10% B	5.1	24.6	5.0	1.5	2.03	4.03	5.591

The ratio (N_{el}/μ_{el}) measured electrically (el) and optically (op) are given in units ($\times$ 10^{29} V s/m^5)

Optoelectronic properties

The experimentally corrected normal transmittance $T(\lambda)$ of the prepared B-doped CdO films grown on corning glass substrate in the UV–Vis–NIR region (400–3000 nm) are presented in Fig. 4. It is clear that the maxima (λ_m) of the transmittance $T(\lambda)$ spectra are in the NIR region; i.e. in the range 1700–1900 nm. For undoped CdO, the wavelength λ_m is 1710 nm and shifted to longer wavelengths with boron doping. In addition, the high-wavelength side of the transmittance curves $T(\lambda)$ of the doped CdO samples shows a clear damping due to the high density of free electrons [31] such that the $T(\lambda)$ curves become like Gaussian NIR filters; this form might find some practical applications.

The normal reflectance in UV, VIS and NIR shown in Fig. 4 for all the investigated samples is almost constant and close to each other in magnitude of less than 1%. The spectral absorption coefficient $\alpha(\lambda)$ is related to the absorbance $A(\lambda)$ by $A(\lambda) = \alpha(\lambda)\, d$, where d is the film's thickness. The absorbance $A(\lambda)$ can be calculated directly from the experimental data using the following equation [32]: $A(\lambda) = \ln[(1-R)/T]$.The optical band gap E_g is evaluated according to the well-known energy-exponential relation [33]:

$$A\,E = B_{op}\,(E - E_g)^m \qquad (1)$$

where B_{op} is the film's constant and the exponent m is equal to 0.5 or 2 for direct or indirect transitions, respectively. Thus, the extrapolation of the plot of $(AE)^2$ versus E for any sample, as shown in Fig. 5 gives the values of its direct band gap (Table 2). For undoped CdO, the band gap obtained is in the range (2.2–2.6 eV), which is known for undoped CdO films prepared by different techniques [1, 34]. Figure 6 shows graphically the variation of E_g with boron doping. Thus, the band gap of CdO decreases by

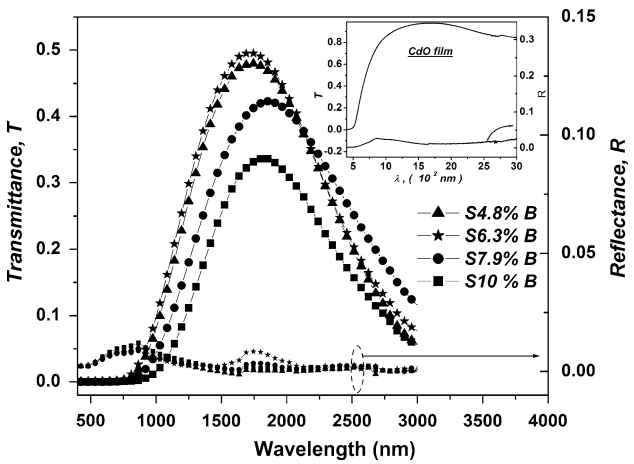

Fig. 4 The optical transmittance and reflectance of the undoped (*inset*) and B-doped CdO films deposited on glass substrates

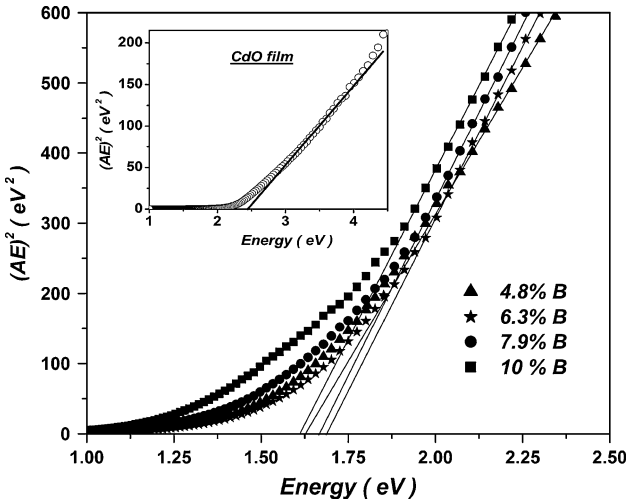

Fig. 5 Calculated (points) energy dependence of spectral optical absorbance (A) in Tauc plot for undoped (*inset*) and B-doped CdO. The *lines* determine the direct band gaps

boron doping. It is interesting to mention here that the band gap of ZnO increases with boron doping [14, 35] although boron ion is also smaller than zinc ion. Thus, the ionic radius of dopant ion is not only the factor that controls the variation of band gap. It was observed that the narrowing of CdO band gap due to B-doping is accompanied with the increasing in carrier concentration. Such observation is in contrast with the Moss–Burstein (B–M) effect or band gap widening (BGW) [36].

Physically, the BGN in heavy donor doping may be ascribed to the following effects. The change in electron–host ions interaction and opening of electron–ionized impurity interaction cause conduction-band renormalization effects and impurity band tailing broadening that finally leads to mergence of the impurity band with the conduction band causing decrease in the effective optical band gap E_g [37, 38].

Phenomenologically, it is possible to correlate the band gap variations with the carrier concentration by considering both BGW and BGN. The BGW is given by BGW $= S_{BGW} N_{el}^{2/3}$ [36], where $S_{BGW}^{th} = 1.348 \times 10^{-18}$ eV m^2. The BGN is given by BGN $= \left(S_{BGN}^{(1)} N_{el}^{2/3} + S_{BGN}^{(2)} N_{el}^{1/3}\right)$, where $S_{BGN}^{(1)} = 4.49 \times 10^{-19}$ eV m^2 and $S_{BGN}^{(2)} = 2.836 \times 10^{-9}/\varepsilon_r$ [11, 39, 40]. The effective dielectric constant ε_r can be considered as $\varepsilon_r = \alpha\,\varepsilon_\infty$, where α is a film's parameter that might comes from the non-parabolic band effects and ε_∞ is long-wavelength dielectric constant that equals about $\varepsilon_\infty = n^2 = 1.6^2$ for pure CdO. Thus,

$$\Delta E_g = E_g - E_{g0} = \text{BGW} - \text{BGN} = S_{BGW,BGN} N_{el}^{2/3} - S_{BGN}^{(2)} N_{el}^{1/3} + C_f \qquad (2)$$

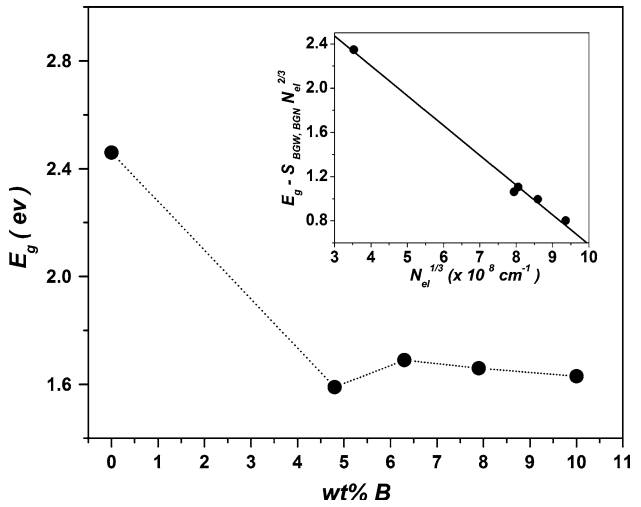

Fig. 6 Variation of band gap (E_g) with doping level of B-doped CdO films. The *inset* shows the dependence of the optoelectronic function $\left(E_g - S_{BGW,BGN} N_{el}^{2/3}\right)$ on the carrier concentration $N_{el}^{1/3}$. The straight line represents the best fit according to Eq. 2

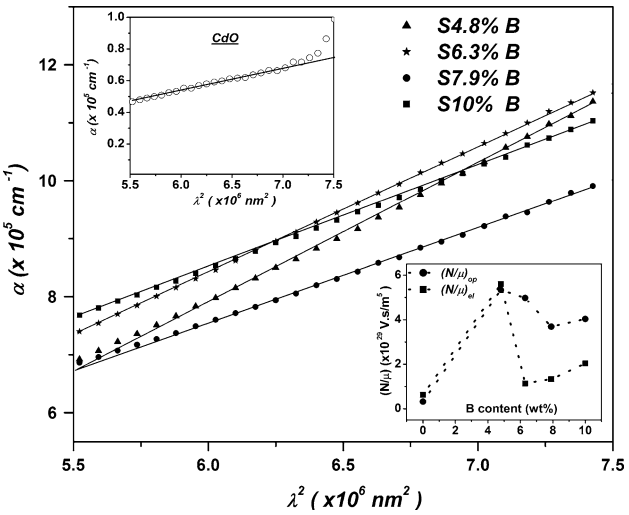

Fig. 7 Dependence of absorption coefficient, α on λ^2 in NIR spectral region for undoped (*inset*) and B-doped CdO films. The *second inset* shows the dependence of the (N_{el}/μ) ratio measured, optically (op) and electrically (el), on the doping level of B-doped CdO films

where C_f is a fitting parameter and $S_{BGW,BGN} = S_{BGW} - S_{BGN}^{(1)} = 8.98 \times 10^{-19}$ eV m^2. Straight line was obtained by plotting $[E_g - S_{BGW,BGN} N_{el}^{2/3}]$ versus $N_{el}^{1/3}$, as shown in the inset of Fig. 6, with $S_{BGN}^{(2)} = 2.69\times 10^{-9}$ eV m, thus $\alpha = 0.41$. The experimental and theoretical orders of magnitudes of $S_{BGN}^{(2)}$ are identical.

Near the threshold of absorption region at NIR ~ 2000 nm, the absorption coefficient is almost linearly proportional to the B-doping level, as given in Table 2. However, it is well known that the absorption in the NIR spectral region is mainly caused by the free carriers [41], which can be studied in the framework of classical Drude theory [42]. For the long-wavelength side of $T(\lambda)$ spectra, i.e. for$\lambda > \lambda_m$, the absorption coefficient α is related to the wavelength according to the following relation [41, 43]:

$$\alpha = \frac{e^3 N}{4\pi^2 c^3 n \varepsilon_0 m_e^{*2} \mu} \lambda^2 = 5.243 \times 10^{-13} \frac{N}{n \gamma^2 \mu} \lambda^2 \qquad (3)$$

in SI system where c is the speed of light, n is the refractive index at NIR region ($n = 1.6$), ε_0 is the permittivity of free space, and e, N and μ are the electronic charge, density and mobility, respectively. For pure CdO, the reduced effective mass m_e^* is equal to γm_e, where $\gamma = 0.274$ and m_e is the free-electron mass [44]. By neglecting of small variations of n in the NIR, a linear α versus λ^2 relationship should be observed, as shown in Fig. 7. Thus, it is possible to estimate the ratio $(N/\mu)_{op}$ (i.e. measured optically) and the results are given in Table 2. The difference between $(N/\mu)_{op}$and $(N/\mu)_{el}$ values comes from different conduction mechanisms and accumulation of boron (or boron oxide) on crystallite boundaries, which can be clearly observed for doping level more than 6.3%. However, the trends of $(N/\mu)_{op}$ and $(N/\mu)_{el}$ variation with boron doping level are almost similar to each other (inset of Fig. 7).

Conclusions

The structural, optical and dc-electrical properties of boron-doped CdO films grown on glass substrates were investigated. The structure and electrical studies show that some of doped B^{3+} ions occupy locations in interstitial positions and/or Cd^{2+}-ions vacancies of CdO lattice. It was observed that doping with B^{3+} ions shrinks the band gap by 30–38% and compresses the host CdO unit cell by 0.1–0.3% compare to undoped CdO. The band gap narrowing was analysed according to available models. All the prepared B-doped CdO films show degenerate semiconducting behaviour. However, the conduction parameters (dc-conductivity, carrier concentration and mobility) were found to improve with boron doping. The utmost improvement of conduction parameter takes place with 7.9 wt% boron doping so that the conductivity increases by about 130 times, mobility by about 7 times and electronic concentration by about 15 times compare to undoped CdO film. We emphasize here that the largest carrier mobility (45–47 cm^2/V s) was found with 6–8% boron doping. From infrared transparent-conducting oxide (IR-TCO) point of view, boron is sufficiently effective for CdO

donor doping. Some phenomenological evaluation of the dependence of band gap on the carrier concentration of samples is discussed

Acknowledgement The author is grateful to Dr. K. I. Jassem and Ms. Hanan Khalifa from Central Labs/College of Science/SEM laboratory.

References

1. Zhao Z, Morel DL, Ferekides CS (2002) Thin Solid Films 413:203
2. Lewis BJ, Paine DC (2000) Mater Res Soc Bull 25:22
3. Yan M, Lane M, Kannewurf CR, Chang RPH (2001) Appl Phys Lett 78:02342
4. Dou Y, Egdell RG, Walker T, Law DSL, Beamson G (1998) Surf Sci 398:241
5. Carballeda-Galicia DM, Castanedo-Perez R, Jimenez-Sandoval O, Jimenez-Sandoval S, Torres-Delgado G, Zuniga-Romero CI (2000) Thin Solid Films 371:105
6. Chopra KL, Ranjan S (1993) Thin film solar cells. Plenum Press, New York
7. Powder diffraction file, joint committee for powder diffraction studies (JCPDS) file No. 05-0640
8. Dakhel AA (2008) Phys Status Solidi A 205:2704
9. Gupta RK, Ghosh K, Patel R, Mishra SR, Kahol PK (2009) Curr Appl Phys 9:673
10. Shu S, Yang Y, Medvedova JE, Ireland JR, Metz AW, Ni J, Kannewurf CR, Freeman AJ, Tobin TJ (2004) J Am Chem Soc 126:13787
11. Dakhel AA (2010) Thin Solid Films 518:1712
12. Dakhel AA (2009) J Alloys Compd 475:51
13. Dakhel AA (2009) Sol Energy 83:934
14. Gao L, Zhang Y, Zhang J, Xu K (2011) Appl Surf Sci 257:2498
15. Pawar BN, Cai G, Ham D, Mane RS, Ganesh T, Ghule A, Sharma R, Jadhava KD, Han S (2009) Sol Energy Mater Sol Cells 93:524
16. Zhao S, Zhou Y, Liu Y, Zhao K, Wang S, Xiang W, Liu Z, Han P, Zhang Ze, Chen Z, Lu H, Jin K, Cheng B, Yang G (2006) Appl Surf Sci 253:726
17. Morales J, Sanchez L (1999) Solid State Ion 126:219
18. Hanamoto K, Sasaki M, Miyatani K, Kaito C, Miki H, Nakayama Y (2001) Nucl Instrum Methods Phys Res B 173:287
19. Lou X, Zhao X, He X (2009) Sol Energy 83:2103
20. Shannon RD (1976) Acta Crystallogr A 32:751
21. Zhao Y, Chen X, Chang X, Zuo J, Li M (2007) Acta Crystallogr E 63:i50
22. Prewitt CT, Shannon RD (1968) Acta Crystallogr B 24:869
23. Gurr GE, Montgomery PW, Knutson CD, Gorres BT (1970) Acta Crystallogr B 26:906
24. Lonsdale TD, Whitaker A (1978) J Mater Sci 13:1503. doi: 10.1007/BF00553206
25. Laureiro Y, Veiga ML, Lopez ML, Garcia-Martin S, Jerez A, Pico C (1991) Powder Diffr 6:28
26. Weil M (2003) Acta Crystallogr E 59:i95
27. Ihara M, Krogh-Moe J (1966) Acta Crystallogr 20:132
28. Kaelble EF (ed) (1967) Handbook of X-rays for diffraction, emission, absorption, and microscopy. McGraw-Hill, New York, p 5
29. Liu H, Mao HK, Somayazulu M, Ding Y, Meng Y, Hausermann D (2004) Phys Rev B 70:094110
30. Zhao TT, Yang T, Yao B, Cong CX, Sui YR, Xing GZ, Sun Y, Su SC, Zhu H, Shen DZ (2010) Thin Solid Films 518:3289
31. Dakhel AA (2009) Mater Chem Phys 117:284
32. Hong WQ (1989) J Phys D Appl Phys 22:1384
33. Tauc J, Abelesn F (eds) (1969) Optical properties of solids. North Holland Publ. Co, Amsterdam
34. Kawamura K, Maekawa K, Yanagi H, Hirano M, Hosono H (2003) Thin Solid Films 445:182
35. Lokhande BJ, Patil PS, Uplane MD (2001) Physica B 302/303:59
36. Pankove JI (1975) Optical processes in semiconductors, P.36. Dover, New York
37. Zhang YZ, Lu JG, Ye ZZ, He HP, Zhu LP, Zhao BH, Wang L (2008) Appl Surf Sci 254:1993
38. Walukiewicz W (1990) Phys Rev B 41:10218
39. Dakhel AA (2011) Curr Appl Phys 11:11
40. Dakhel AA (2010) J Alloys Compd 504:7
41. Qiao Z, Agashe C, Mergel D (2006) Thin Solid Films 496:520
42. Mergel D, Qiao Z (2002) J Phys D Appl Phys 35:794
43. Dakhel AA (2010) Sol Energy 84:1433
44. Asahi R, Wang A, Babcock JR, Edleman NL, Metza W, Lane MA, Dravid VP, Kannewurf CR, Freeman AJ, Marks TJ (2001) In: Proceeding of the international symposium on transparent oxide thin films for electronics and optics, Tokyo, 8–9 Nov